Evolution of the vacuum Rabi peaks in a detuned atom-cavity system

J. Gripp, S. L. Mielke, and L. A. Orozco
Department of Physics, State University of New York at Stony Brook, Stony Brook, New York 11794-3800
(Received 13 May 1997)

We measure the transmission spectrum of an optical cavity filled with two-level atoms. For small intensities, the coupling between atoms and a single mode of the cavity splits the spectrum into two normal modes: the vacuum Rabi peaks. We gradually decouple the system in two ways and study the evolution of the vacuum Rabi peaks. First we lower the atom-cavity coupling frequency through its intensity dependence, showing that the peaks shift, deform, exhibit frequency hysteresis, and eventually merge into a single peak that approaches the empty cavity resonance. Second we detune the atoms and the cavity mode and observe an avoided crossing. The normal modes of the coupled system transform into the two resonances of the uncoupled system. We map out the transition region and find good agreement with theoretical predictions. [S1050-2947(97)07910-9]

PACS number(s): 42.50.−p, 42.65.Pc, 32.80.Bx

I. INTRODUCTION

The spectroscopic properties of atoms coupling to a single mode of a cavity have their origin in the single two-level-atom single-mode theory developed by Jaynes and Cummings [1]. Sánchez Mondragón *et al.* [2] later calculated the spectrum and found a double-peak structure for small numbers of energy quanta in the system and named it the vacuum Rabi splitting. It is caused by the coupling between the atom and the cavity and results in an exchange of energy between the two. Agarwal showed that the structure remained for a collection of N two-level atoms [3]. Most of these findings came from cavity quantum electrodynamics (QED). In parallel, the quantum optics community focused on optical bistability (OB), which is present in the transmission characteristics of a driven single-mode cavity filled with a collection of N two-level atoms (see, for example, the review of Lugiato [4]). As the OB community studied systems with small numbers of atoms and large coupling between atoms and the cavity, the link between cavity QED and OB became more apparent. The study of this system of a small number of atoms interacting with a single mode of the electromagnetic field is now mainly identified with cavity QED (Ref. [5]), but the ample theory and experimental studies of OB help in the understanding of many of the observations.

The experimental study of the vacuum Rabi splitting either in the time domain (energy exchange) or in the frequency domain (transmission spectrum) has been limited to the low-intensity regime, where the amount of excitation in the system is very low. Kaluzny *et al.* [6] observed the energy exchange in experiments with microwave cavities and Rydberg atoms. Brecha *et al.* [7] studied the time response of their optical bistability system observing the exchange between a single mode of an optical cavity and a collection of optically pumped sodium atoms. Several experimental studies of the spectrum followed in the optical regime [8–11]. Recently, we have studied the time response of the atom-cavity system to step excitation without the low-intensity restriction [12], finding agreement with semiclassical predictions. Carmichael [13] has shown formally that the system reduces to a model of two coupled harmonic oscillators in the limit of low excitation. In this regime, quantum-mechanical and semiclassical calculations predict the same spectrum.

Differences arise when the excitation is not small. The quantum-mechanical model predicts multiple resonances caused by the nonuniform spacing of the energy levels in the Jaynes-Cummings ladder, while the semiclassical model shows anharmonic behavior of the vacuum Rabi peaks (see the contribution by Carmichael *et al.* in Ref. [5] and Gripp *et al.* [14]). Two recent experiments have reported the observation of the discrete uneven structure on the Jaynes-Cummings Hamiltonian: Brune *et al.* [15] with Rydberg atoms in microwave cavities and Meekhof *et al.* [16] with an ion in a rf trap. The excitation available in both experiments permits the exploration of more than the first excited state of the system.

Finally, the vacuum Rabi peaks have been studied in semiconductor microcavities [17]. The behavior at low intensities is similar to our observations, although the underlying mechanisms are different.

In this paper we present an experimental study of the evolution of the vacuum Rabi peaks in the optical regime for arbitrary excitation. In our system a collection of two-level atoms couples to a single mode of an interferometer. We start with a maximally coupled system, keeping atoms and cavity on resonance, measuring the vacuum Rabi splitting with a weak excitation. Then we evolve the system gradually in different ways, either by increasing the excitation field, causing a decoupling due to the saturation of the atoms, or by introducing a detuning between atoms and cavity, causing a decoupling because of the frequency mismatch. We map out the transition region between the coupled and the uncoupled system and compare the experimental results with a semiclassical theory.

We are interested in a detailed understanding of the spectral properties of an atoms-cavity system to pursue experiments that study the response of a driven quantum optical system [18] to non-classical light. An efficient coupling between source and receiver is crucial [19,20] and relies on a good matching of the spectral features between the two.

The paper is organized as follows. Section II presents an overview of the theoretical model, starting with the quantum-mechanical description and leading to a semiclassical model

relevant for the experimental conditions. Section III describes the experimental apparatus and the experiments. Section IV shows the results and compares them with the theoretical predictions. Section V summarizes the work and presents the conclusions.

II. THEORETICAL BACKGROUND

We start with the Hamiltonian for an ensemble of N two-level atoms interacting with a single mode of the electromagnetic field of a cavity. The atoms and the cavity field couple to reservoirs (heat baths) and we include a driving field [21]

$$\hat{H}=\hat{H}_0+\hbar\sum_{j=1}^{N} g_j(i\hat{a}^{\dagger}\hat{\sigma}_j^{-}e^{-i\vec{k}\cdot\vec{r}_j}+\text{H.c.})+\hat{H}_R+\hat{H}_D. \quad (1)$$

$\hat{H}_0$ is the uncoupled Hamiltonian of the cavity field (resonant frequency ω_c) and the atoms (transition frequency ω_a). The second term is the energy exchange between the field and atoms at a rate of g_j. $\hat{H}_R$ describes two reservoirs: the atoms coupling through spontaneous emission into other modes of the electromagnetic field and the coupling of the cavity mode with the outside. $\hat{H}_D$ is the excitation through an external classical driving field $\mathcal{E}$ of frequency ω_l. The operators $\hat{a}^{\dagger}$, $\hat{a}$ are the single-mode raising and lowering operators. $\hat{\sigma}_j^{+}$ and $\hat{\sigma}_j^{-}$ are Pauli atomic operators for the individual atom j and g_j is the position-dependent coupling between an atom and the mode of the electromagnetic field. The cavity mode function for the experimentally relevant TEM_{00} Gaussian standing-wave mode is $\psi(\vec{r})=\cos(2\pi z/\lambda)\exp(-r_{\perp}^2/w_0^2)$, with z and $r_{\perp}$ the axial and radial coordinates, λ the wavelength of light, and w_0 the waist of the mode. For the TEM_{00} mode of a standing-wave cavity of length l the mode volume $V=\int|\psi(\vec{r})|^2d^3r=\frac{1}{4}\pi w_0^2 l$. The maximal coupling between a single atom and the mode is $g_0=\mu\sqrt{\omega_a/2\hbar\epsilon_0 V}$, where μ is the transition dipole moment of the atom. The position-dependent coupling rate $g_j(\vec{r})=g_0\psi(\vec{r})$. The effective atomic number [22] is $\overline{N}=\Sigma_{j=1}^{N}|\psi(\vec{r}_j)|^2$.

From the Hamiltonian of Eq. (1) we obtain a master equation by tracing over the reservoirs and making the Born and Markov approximations. The equation describes the time evolution for the atom-cavity system including dissipation. The resulting three decay rates κ, $\gamma_{\perp}$, and $\gamma_{\parallel}$ characterize the cavity, atomic polarization, and atomic inversion dissipations, respectively. The magnitude of the coupling g_0 compared to the dissipation rates κ and $\gamma_{\perp}$ sets our system in the intermediate regime of cavity QED since all three rates are of the same order. The relevance of this is expressed in the single-atom cooperativity C_1 and the saturation photon number n_0 [22]:

$$C_1=\frac{g_0^2}{2\kappa\gamma_{\perp}},\quad n_0=\frac{\gamma_{\perp}\gamma_{\parallel}}{4g_0^2}b. \quad (2)$$

$b=V/\int|\psi(\vec{r})|^4d^3x$ is the dimensionless effective mode volume and depends on the cavity geometry [21]. For a plane-wave ring cavity [$\psi(\vec{r})=1$] $b=1$, while for a Gaussian standing wave $b=\frac{8}{3}$. Roughly speaking, C_1 is a measure of how much one atom contributes to the system dynamics, whereas n_0 determines the number of photons that are needed to encounter nonlinear behavior.

The experimental conditions allow a number of assumptions [4] established in the OB literature that we summarize here. (i) The input radiation couples only into the lowest-order circularly symmetric mode of the cavity (single-transverse-mode approximation [21]). (ii) The single-pass absorption by the atoms and the transmission of the mirrors are small. Additionally, the cavity mode diameter does not vary significantly across the atomic sample. In this case the cavity field can be treated in the uniform field limit [4] where the absorption by the atoms and the transmission of the mirrors go to zero while their ratio remains constant and arbitrary. (iii) The atoms decay from the excited to the ground state only by emitting radiation ($\gamma_{\parallel}=2\gamma_{\perp}$, with $\gamma_{\parallel}=\tau^{-1}$, where τ is the radiative lifetime of the atomic transition). (iv) The field inside the cavity has a standing-wave configuration and the transverse profile has the Gaussian shape of the TEM_{00} mode.

If the presence or absence of one photon or one atom changes the behavior of the system, then atom-cavity correlations cannot be neglected. However, if the number of atoms N and the number of photons n in the system is large, the semiclassical limit ($N\to\infty$, $C_1\to 0$, and $C_1N\to$const; $n\to\infty$, $n_0\to\infty$, and $n/n_0\to$const) becomes valid. We neglect the atom-photon correlations by applying a semiclassical decorrelation replacing $g_j\langle\hat{a}\hat{\sigma}_j^k\rangle$ by $g_j\langle\hat{a}\rangle\langle\hat{\sigma}_j^k\rangle$ in the expectation values calculated from the master equation.

The result is the well-known set of Maxwell-Bloch equations [21] for a collection of two-level atoms interacting with a single mode of the radiation field in a cavity including excitation through a driving field $\mathcal{E}$: the radiation field

$$\frac{d}{dt}\langle\hat{a}\rangle=-\kappa(1+i\theta)\langle\hat{a}\rangle+\sum_{j=1}^{N} g_j\langle\hat{\sigma}_j^{-}\rangle+\mathcal{E},\ \text{and its H.c.}, \quad (3)$$

atomic polarization

$$\frac{\partial}{\partial t}\langle\hat{\sigma}_j^{-}\rangle=-\gamma_{\perp}(1+i\Delta)\langle\hat{\sigma}_j^{-}\rangle+g_j\langle\hat{a}\rangle\langle\hat{\sigma}_j^{z}\rangle,\ \text{and its H.c.}, \quad (4)$$

and atomic inversion

$$\frac{\partial}{\partial t}\langle\hat{\sigma}_j^{z}\rangle=-\gamma_{\parallel}(\langle\hat{\sigma}_j^{z}\rangle+1)-2g_j(\langle\hat{a}\rangle\langle\hat{\sigma}_j^{+}\rangle+\langle\hat{a}^{\dagger}\rangle\langle\hat{\sigma}_j^{-}\rangle). \quad (5)$$

The cavity and atomic detunings θ and Δ are $\theta=(\omega_c-\omega_l)/\kappa$ and $\Delta=(\omega_a-\omega_l)/\gamma_{\perp}$. It is convenient to rescale these equations such that in the dispersive limit ($\Delta\gg 1$) the steady-state behavior is independent of the mode function [21]. For this purpose we introduce a normalized input field $y=\mathcal{E}/(\kappa\sqrt{n_0})$ and a normalized output field $x=\langle\hat{a}\rangle/\sqrt{n_0}$ and replace the sum over the atoms by an integral over the mode function $\Sigma_{j=1}^{N}f(\psi(\vec{r}_j))\to\overline{N}/V\int f(\psi(\vec{r}))d^3r$, which is valid in the case of a uniform atom distribution with a large number of atoms. The normalized input and output intensities are directly related to the normalized fields. Respectively, they are $X=|x|^2$ and

$Y=|y|^2$. The definition of the cooperativity C, the critical parameter for OB, shows explicitly the relationship with the parameters of cavity QED

$$C=C_1\overline{N}=\frac{g_0^2\overline{N}}{2\gamma_\perp\kappa}. \tag{6}$$

The stationary solution of the Maxwell-Bloch equations is the state equation

$$y=x[(1+2C\chi)+i(\theta-2C\Delta\chi)]. \tag{7}$$

In the case of a plane-wave ring cavity, $\chi=1/(1+\Delta^2+|x|^2)$. For the experimentally relevant case of a standing-wave mode with Gaussian beam profile

$$\chi=\frac{3}{2|x|^2}\ln\left[\frac{1}{2}+\frac{1}{2}\sqrt{1+\frac{8|x|^2}{3(1+\Delta^2)}}\right]. \tag{8}$$

Equations (7) and (8) are the starting point for the theoretical results presented in the following sections and in the data analysis.

In the limit of low excitation, the atom-cavity system behaves like two coupled harmonic oscillators. In the quantum picture, the cavity by itself is a quantized harmonic oscillator with an infinite number of equally spaced energy levels. The atoms by themselves have only two energy levels, but as long as the driving field is weak, the atoms behave like harmonic oscillators. Formally, this correspondence has been shown by Carmichael [13], using the Schwinger representation of a two-level atom in terms of two boson operators. The first operator creates or destroys an exited state and the second operator creates or destroys a ground state. This approach is only valid if the excited state is sparsely populated. The dipole coupling lifts the mode degeneracy between cavity and atoms. The combined system has two normal modes with a mode splitting of twice the coupling frequency. Without atom-cavity detuning the displacement of these modes from atomic resonance is given by

$$\Omega_{VR}=g_0\sqrt{\overline{N}.} \tag{9}$$

The splitting survives dissipation as long as the decay rates κ and $\gamma_\perp$ are small compared to the rate of energy exchange Ω_{VR}. It is easy to fulfill this condition in the intermediate regime of cavity QED with N atoms, as has been observed by several groups [8–11,14,23].

In order to gain some insight into the problem, we focus on a model with a traveling plane-wave cavity. We use the optical bistability state equation (7) and calculate the ratio of transmitted to incident field as a function of probing frequency Ω:

$$\left|\frac{x}{y}\right|^2=\left|\frac{\kappa(\gamma_\perp+i\Omega)}{(\kappa+i\Omega)(\gamma_\perp+i\Omega)+\dfrac{g_0^2\overline{N}}{1+\gamma_\perp^2|x|^2/(\gamma_\perp^2+\Omega^2)}}\right|^2. \tag{10}$$

To stress the coupling between the atoms and the cavity, the transmission may be written as consisting of two parts related to the two normal modes of the system [24], each one centered on $\Omega_{1,2}$:

$$\left|\frac{x}{y}\right|^2=\left|\frac{A}{i\Omega+\Omega_1}+\frac{B}{i\Omega+\Omega_2}\right|^2, \tag{11}$$

where

$$A=\kappa\frac{\gamma_\perp+\Omega_1}{\Omega_1-\Omega_2}, \tag{12}$$

$$B=\kappa\frac{\gamma_\perp+\Omega_2}{\Omega_2-\Omega_1}, \tag{13}$$

and

$$\Omega_{1,2}=-\frac{\kappa+\gamma_\perp}{2}\pm i\sqrt{-\left(\frac{\kappa-\gamma_\perp}{2}\right)^2+\frac{g_0^2\overline{N}}{1+\dfrac{\gamma_\perp^2|x|^2}{\gamma_\perp^2+\Omega^2}}}. \tag{14}$$

This expression reveals the conditions for the observation of an oscillatory exchange of energy. The imaginary part of $\Omega_{1,2}$ has to be positive, so $g_0\sqrt{\overline{N}}$ has to be larger than the difference between the dissipation rates. Equation (14) reduces to Eq. (9) in the limit of no dissipation and weak excitation $x\to 0$. We can make a series of observations about the behavior of the peaks: In the semiclassical picture, the normal modes of the system are the eigenvalues of the Maxwell-Bloch equations [25] in the weak-field limit. The positions of the vacuum Rabi peaks can be obtained either from the eigenvalues of the Maxwell-Bloch equations or from Eq. (14). In the weak-field limit, we identify the imaginary part of $\Omega_{1,2}$ with the coupling between the atoms and the cavity. We see that the coupling rate decreases as the intensity inside the cavity increases. The atoms cease to behave in a cooperant fashion and respond more and more as single atoms until they reach saturation and cease to have a significant effect on the transmission. In the limit of high excitation ($|x|^2\gg 1$), the atoms are saturated and play no important role in the atom-cavity system. The imaginary part of $\Omega_{1,2}$ becomes real and the transmission, characterized by the real part of $\Omega_{1,2}$, resembles that of an empty cavity. This intensity dependence causes the evolution of the vacuum Rabi peaks from a doublet to a singlet.

An optics explanation of the semiclassical picture is given by Refs. [9,24]. The atoms act as a medium where the index of refraction causes a phase shift. If the laser frequency is detuned by the right amount, then the frequency shift caused by the cavity will compensate for the atomic phase shift and the transmission will be enhanced due to constructive interference. For small input intensities and small atom-cavity detunings this zero-phase shift condition can be met at three frequencies. The center one is on resonance, but the transmission is heavily suppressed by the atomic absorption. The remaining two transmission peaks correspond to the vacuum Rabi peaks.

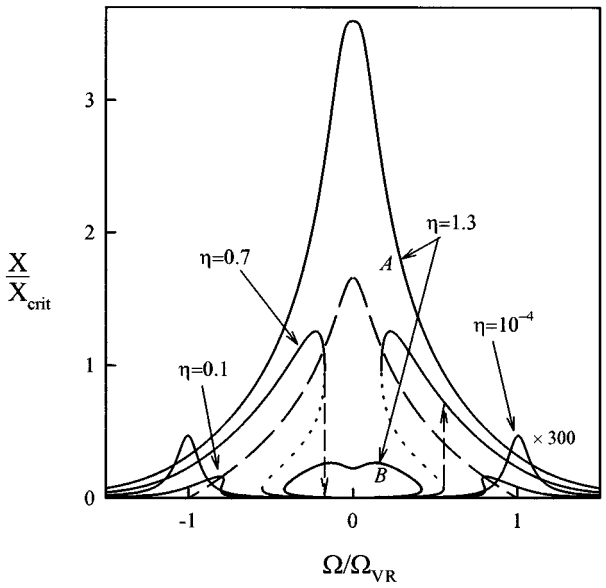

FIG. 1. Evolution of the two vacuum Rabi peaks depending on the input intensity $\eta = Y/Y_{crit}$. The solid curves are solutions of the state equation (7) and the dashed curve is the zero-phase condition (16).

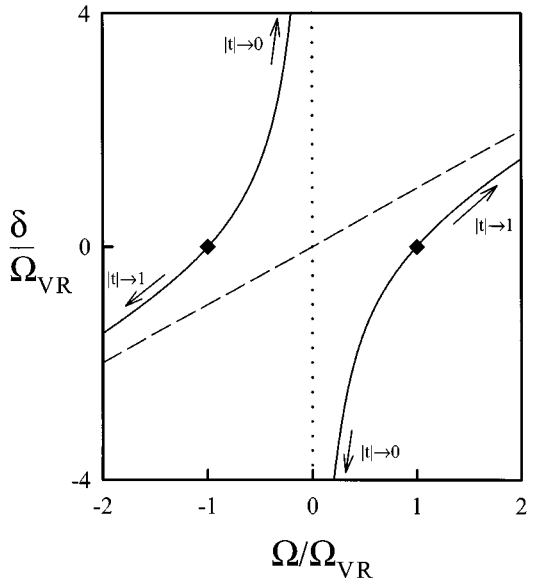

FIG. 2. Avoided crossing between atoms and cavity. The solid curves show the solution of the zero-phase condition. The diamonds mark the position of the vacuum Rabi peaks without atom-cavity detuning. The dotted curve (atoms) and the dashed curve (cavity) are the eigenfrequencies of the uncoupled system ($g_0 = 0$). $(\Omega_{VR}, \kappa, \gamma_\perp) = (35.5, 3.0, 3.0) \times 2\pi \times 10^6$ rad/s.

We calculate the position of the peaks according to this zero-phase condition from Eq. (7) without atom-cavity detuning. In the traveling plane-wave model

$$\Omega_{ZP}^{PW} = \pm \gamma_\perp \sqrt{\frac{g_0^2 \overline{N}}{\gamma_\perp^2} - 1 - X} \tag{15}$$

and in the Gaussian standing-wave model

$$\Omega_{ZP} = \pm \gamma_\perp \sqrt{\frac{8X}{3\left\{\left[2\exp\left(\frac{2\gamma_\perp^2 X}{3g_0^2 \overline{N}}\right) - 1\right]^2 - 1\right\}} - 1}. \tag{16}$$

These two expressions are valid as long as the intensity X is small enough to have a real Ω_{ZP}. The exact location of the peak of the cavity transmission is slightly different from the prediction of the zero-phase model or the pure vacuum Rabi frequency, but for the experimental parameters of our experiment the differences are less than 2% [26].

Figure 1 shows the evolution of the vacuum Rabi peaks together with the zero-phase condition for zero atom-cavity detuning ($\omega_a = \omega_c$) in the Gaussian standing-wave model as a function of the scaled laser detuning $\Omega/\Omega_{VR} = (\omega_a - \omega_l)/\Omega_{VR}$ for different input intensities. The output intensity is normalized to X_{crit}, the smallest value at which the atoms can remain saturated when they are driven on resonance. This corresponds to the value at which the system jumps from the upper to the lower branch in the on-resonance optical bistability curve; it is the lower limit of the region of on-resonance bistability. Y_{crit} is the input intensity that corresponds to the output intensity X_{crit}.

For small input intensities $\eta = Y/Y_{crit} = 10^{-4}$, the transmission spectrum shows the two vacuum Rabi peaks. When the driving intensity is increased, the atoms begin to saturate and the peaks shift their position and deform. They become anharmonic oscillators and bend towards the center, where they eventually meet once the input intensity is large enough. At intermediate input intensities the solution of the state equation (7) has three output intensity values within a certain range of the laser detuning. For $\eta = 0.7$ the dotted curves show the region of instability and the two vertical dashed arrows indicate where a scan from lower to higher frequencies would jump from the upper to the lower branch and back. For high intensities ($\eta = 1.3$) there are two separate solutions, the regular one-peaked spectrum A and a cave B, the bottom half of which can be reached as shown in Fig. 7. The parameters for this plot are $C = 70$, $(\kappa, \gamma_\perp, g_0) = (3.0, 3.1, 2.5) \times 2\pi \times 10^6$ rad/s, $X_{crit} = 390$, and $Y_{crit} = 2500$. The evolution from two coupled harmonic oscillators at low intensity to highly deformed anharmonic oscillators is visible in Fig. 1. A more detailed study of this anharmonicity is found in Ref. [24].

The efficiency of the coupling between atoms and cavity decreases when the atom-cavity detuning is not zero but of a finite value $\delta = \omega_a - \omega_c$. This affects the position and height of the peaks.

Figure 2 shows the position of the transmitted peaks, as a function of the atom-cavity detuning δ for small intensities. The two diamonds mark the position of the vacuum Rabi peaks in the on-resonance case ($\delta = 0$). When the detuning increases, the atom-cavity system decouples and the peaks (solid curves) approach asymptotically the eigenfrequencies of the atoms (dotted curve) and the cavity (dashed curve). This evolution is described by the zero-phase condition

$$\lim_{X\to 0}\delta=\Omega\left(1-\frac{\Omega_{VR}^2}{\gamma_\perp^2+\Omega^2}\right). \tag{17}$$

The result is an avoided crossing [24,25] with a minimum separation of $2\Omega_{VR}$.

The peak heights are affected since the two components of the decoupled system act differently in transmission. We define the transmission as $|t|^2=X/Y$ for X at the peak maximum. In the on-resonance case ($\delta=0$) both vacuum Rabi peaks have a value of

$$|t|^2=\left(\frac{\kappa}{\kappa+\gamma_\perp}\right)^2. \tag{18}$$

For small detuning $|\delta|\ll\Omega_{VR}$, the transmission of the left (right) vacuum Rabi peak at $-\Omega_{VR}$ ($+\Omega_{VR}$) depends approximately on δ in the form

$$|t|_{l,r}^2\approx\left[\frac{\kappa}{\kappa+\gamma_\perp}\left(1\pm\frac{\delta}{\Omega_{VR}}\frac{\gamma_\perp}{\kappa+\gamma_\perp}\right)\right]^2. \tag{19}$$

For large positive detuning ($\delta\gg\Omega_{VR}$), the left peak disappears ($|t|\to 0$) and the right peak reaches the value of the empty cavity transmission ($|t|\to 1$). The behavior is reversed for negative detuning, as indicated in Fig. 2.

In terms of measured quantities the intensities corresponding to the normalized fields are

$$Y=\frac{3P_{in}}{\pi w_0^2 I_{sat}}\frac{T_0}{T_2},\quad X=\frac{3P_{out}}{\pi w_0^2 I_{sat}}\frac{1}{T_2}. \tag{20}$$

Here P_{in} and P_{out} are the incident and transmitted powers and $I_{sat}=\pi hc/3\tau\lambda^3$ is the saturation intensity.

The transmissivity of the exit mirror is T_2. The enhancement factor of the cavity T_0/T_2 takes into account the presence of other losses in the cavity due to absorption and scattering on the mirrors. These losses give an overall cavity transmission T_0 of less than unity.

III. EXPERIMENT

A. Apparatus

The heart of this experiment consists of a single-mode optical cavity placed inside a vacuum system, traversed by a collimated thermal beam of optically pumped rubidium. Two spherical mirrors 1.2 cm in diameter separated by 1.9 mm form the cavity. The mirrors are custom coated by Research-Electro-Optics Inc.; they have a transmission of $T=232\times 10^{-6}$ and much lower scatter losses. We achieve an on-resonance cavity transmission of $T_0=0.80$. Two piezoelectric transducers (PZT's), mounted inside a stainless-steel tube, hold the mirrors. The tube rests on layers of Sorbothane and lead inside the vacuum system. The vibration isolation given by this setup enables us to compensate with an electronic lock for thermal drifts and residual vibrations. When the lock is interrupted, the cavity stays within a fraction of the cavity linewidth for tens of milliseconds. Both mirrors have a radius of curvature of 7.5 cm. The TEM_{00} mode has $w_0=45$ μm and a longitudinal mode spacing of 80 GHz. An atom with an average velocity of 400 m/s crosses the beam waist ($2w_0$) in approximately nine lifetimes. The next-order transverse mode is 5.7 GHz away. To eliminate the effects of higher-order modes, we mode match 95% of the light intensity into the TEM_{00} mode. We achieve a good experimental realization of the theoretical ideal of a single-mode cavity. The single atom-cavity coupling for this system is $g_0=2.6\times 2\pi\times 10^6$ rad/s with a cavity decay rate of $\kappa=3.1\times 2\pi\times 10^6$ rad/s.

The vacuum system is pumped by an oil diffusion pump and consists of a stainless-steel chamber and a series of commercially available components. We produce the atomic beam with an effusive oven and a set of collimating apertures. The divergence angle is 4×10^{-3} rad, limiting the Doppler shift to less than 0.9 MHz. Liquid-nitrogen cold traps keep the rubidium background low; the pressure in the chamber is 10^{-5} Pa. All measurements are done with the more abundant ^{85}Rb isotope. The atomic beam enters the cavity perpendicular to the cavity mode to avoid Doppler broadening. For the on-resonance measurements (Sec. IV A), the effective atom number is 220. The experiments with atom-cavity detuning (Sec. IV B) are carried out with an effective atom number of 100. Before the atoms enter the cavity, they are optically pumped with circularly polarized light from a diode laser into the $^5S_{1/2}$, $F=3$, $m_F=3\to{}^5P_{3/2}$, $F=4$,$m_F=4$ two-level cycling transition. The atomic decay rate of the excited state is $\gamma_\perp=3.05\times 2\pi\times 10^6$ rad/s. A magnetic field of 10^{-4} T defines an axis of quantization parallel to the optical axis and keeps the atoms in the correct state while they travel 2 cm from the optical pumping region into the cavity. Along this way, the magnetic field is uniform to within $\pm 5\times 10^{-7}$ T. We employ a second diode laser as a repumper for the $^5S_{1/2}$, $F=2$, $m_F=2\to{}^5P_{3/2}$, $F=3$, $m_F=3$ transition.

Figure 3 shows the experimental setup. The main excitation source is a Coherent 899-01 titanium sapphire (Ti:sapphire) ring laser. Two frequency narrowed Sharp LT024 diode lasers serve various purposes such as optically pumping and repumping the atomic beam. The light of the Ti:sapphire laser is split into two parts: one goes to a frequency lock and diagnostic setup for the laser and the other to the experiment. The light sent into the lock and diagnostic setup is frequency modulated at 12 MHz with a New Focus 4001 electro-optic modulator (EOM) and then shifted with two acousto-optic modulators (AOM's), the first one in double-pass and the second one in single-pass configuration. We derive an error signal from an FM saturation spectroscopy setup in a rubidium cell (Pound-Drever-Hall lock [27]). This signal allows us to lock the laser to peaks in the shifted rubidium spectrum. The spectrum also serves for the calibration of the frequency of the laser detuning. For the on-resonance experiments (Sec. IV A) we choose the rf of the double-pass AOM and the peak in the rubidium spectrum such that the light going into the cavity is on resonance with the atoms. The Ti:sapphire laser scans around this resonance frequency over an interval of 180 MHz.

We split the light going to the experiment into a cavity lock beam and a probe beam. A variable attenuator controls the intensity of the circularly polarized and mode-matched probe beam, ranging from less than a nanowatt to hundreds of nanowatts. The more intense lock beam (a few milliwatts) is frequency modulated at 11 MHz and sent through a me-

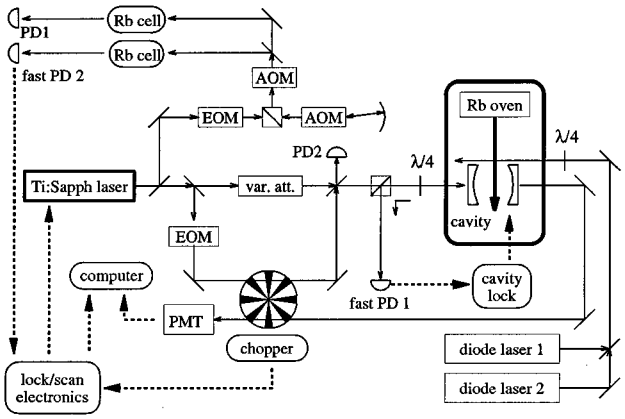

FIG. 3. Experimental setup. In the interaction region, the atomic rubidium beam encounters two laser beams. First a circularly polarized beam from two diode lasers optically prepumps and repumps the ^{85}Rb atoms into the two-level transition. Then they enter the cavity and interact with the second beam, derived from the Ti:sapphire laser. This beam is intensity controlled by a variable attenuator, circularly polarized and mode matched to the TEM_{00} mode of the cavity. The cavity lock (fast PD 1) uses the back reflection of a chopped and FM modulated beam. The frequency of the Ti:sapphire laser is controlled with a rf saturation spectroscopy setup (fast PD 2) and can be adjusted using a double-pass acousto-optic modulator (AOM).

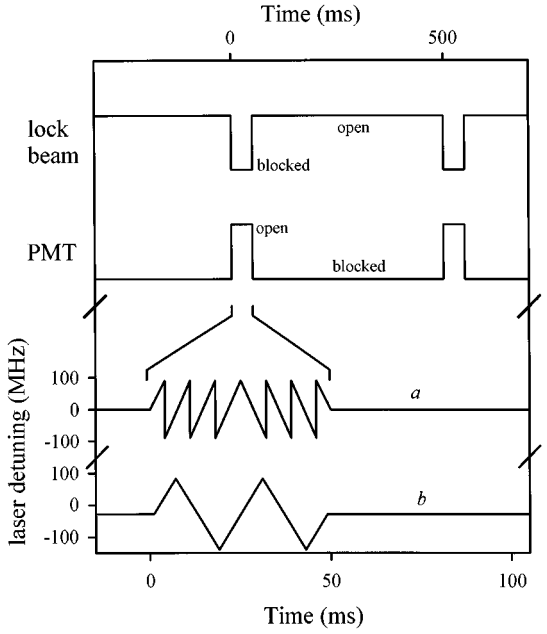

FIG. 4. Timing sequence used in the experiment. *a* shows the laser frequency for on-resonance measurements and *b* shows one example of the off-resonance measurements ($\delta = -29\times 2\pi\times 10^6$ rad/s).

chanical chopper wheel before being recombined with the probe beam and entering the cavity. A fast photo diode with 60 dB amplification measures the back-reflected lock beam and supplies the signal for another Pound-Drever-Hall lock. The output of the cavity goes through the same mechanical chopper but at a different position and then into a photomultiplier tube (PMT). The chopper wheel allows only one of the beams to pass at any point in time. Figure 4 shows the chopper timing and frequency ramping sequence. The cycle time is determined by the scanning ratio of the laser frequency and the need to ensure steady-state behavior of the system. The chopper blocks the lock beam for 75 ms and passes it for 425 ms. The beam going from the cavity to the PMT passes for 64 ms within the 75-ms window and is blocked during the remaning 436 ms. The experiments with atom-cavity detuning (Sec. IV B) require some modifications in the setup. Two mechanical shutters replace the chopper wheel. By synchronously driving a scanable étalon and a PZT mirror inside the Ti:sapphire laser we extend the scanning range from 180 MHz to 1 GHz.

B. Procedure

We perform each set of measurements in two steps. First, we heat up the oven slowly and monitor the intensity input-output behavior of the atom-cavity system by ramping the input intensity on-resonance up and down. When the effective atom number is large enough ($\approx$220), a well-defined intensity hysteresis appears with a ratio of 2 for the input intensity of the switching points. We leave the oven temperature at this level during the experiment.

From the position of the switching points we measure the size of the bistability and determine the cooperativity as a function of the ratio of the switching points [28]. To serve as a guide, we can use Eq. (6) to calculate the expected value of $g_0\sqrt{N}$ and later compare it to the measured value [22]. The absolute position of the switching points tells us about the input intensity levels that have to be used to measure the evolution of the vacuum Rabi peaks.

Second, we stop the intensity scan and perform transmission measurements for a series of fixed input intensities by scanning the frequency of the laser. The cavity is held on resonance with the atoms using an alternating locking-probing scheme (see Fig. 4). The chopper wheel rotates with a frequency of 2 Hz.

When the lock beam turns off and the PMT opens, we scan the frequency of the probe beam six times over a range of 180 MHz, three times from lower to higher frequencies and three times from higher to lower frequencies. The cavity is left without feedback during the scan period.

We collect data with a data acquisition board with 12-bit analog-to-digital converters to read two time-varying signals directly into a computer: the PMT signal from the cavity output, amplified with a calibrated dc to voltage amplifier, and the rubidium spectrum from the saturation spectroscopy setup used for frequency calibration. Additionally, we record three signals that stay constant during a scan: the input intensity, the temperature of the oven, and the fluorescence of the interaction region between the optical pumping beam and atomic beam. We also record the time varying signals into a digital storage oscilloscope.

We take scans with different values for the intensity of the probe beam both below and above Y_{crit}. We measure the input intensity by sending part of the input beam into a photodiode (PD2 in Fig. 3), which we calibrate with a NIST traceable power meter. The output beam goes into the PMT with discrete gain settings, each of which we also calibrate with the power meter. The power meter has an accuracy of

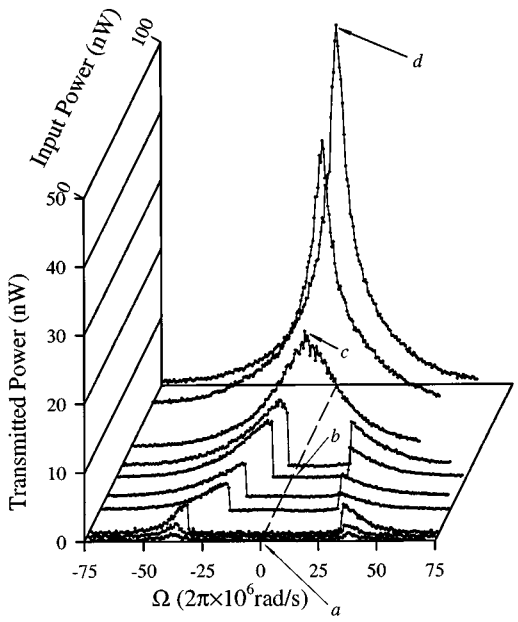

FIG. 5. Transmitted spectrum as a function of the excitation power. The atom-cavity detuning is zero for all scans. The frequency is scanned from below to above atomic resonance. The heights of the three scans with lowest intensities have been multiplied by a factor of 5. Scan *b* is shown in detail in Fig. 6. The arrows *a*, *b*, *c*, and *d* indicate the corresponding points in Fig. 7. The scaled input intesitites η are 0.02, 0.76, 1.09, and 1.84, respectively. The data of Figs. 5 and 7 were taken during the same run.

5%. For consistency, we use the measured input power and the transmission of the empty cavity as a second way of calibrating the output power. Although the voltage driving the PZT of the laser varies linearly in time, nonlinearities in the response can affect the linearity of the laser scan. We use the signal of the saturation spectroscopy setup to obtain a calibration of the frequency axis. The jitter in the laser scan is less than ± 3 MHz across the scanned range.

For the measurements with atom-cavity detunings, we start out in the same way, by fixing the oven temperature at a value that leads to a visible on-resonance hysteresis. This time the effective atom number is 100. Then we scan the frequency of the Ti:sapphire laser, keeping the intensity fixed. We scan once back and forth over a range of up to 400 MHz every lock-probe cycle. We first measure the on-resonance response and next we detune the lock beam, which results in an equal detuning between the cavity and the atoms. Again we record transmission spectra for a variety of different input intensities and atom-cavity detunings. We extract the frequency information from the rubidium spectra. A fit to the entire spectrum shows that the frequency uncertainty is less than ± 3 MHz in the center of the scan ($|\Omega| < 50 \times 2\pi \times 10^6$ rad/s) and less than ± 5 MHz for larger laser detunings ($|\Omega| > 50 \times 2\pi \times 10^6$ rad/s).

IV. RESULTS

A. Resonant atom-cavity system

Figure 5 shows our transmission measurements for the resonant atom-cavity system. There is a large amount of information in this figure. We have analyzed it in a preliminary way in Ref. [14]. Figure 5 shows a doublet evolving into a singlet as the driving intensity increases from scan to scan. All the scans displayed go from lower to higher laser detunings. The driving intensity changes from low (trace *a*) to high (trace *d*). A thin curve connects all the consecutive data points of a given scan to guide the eye. We begin the analysis by focusing on the frequency positions of the peaks. In this case the connection between theory and experiment is immediately given by the position of the peak maxima and the theoretical values obtained from the zero-phase condition (16). This approach requires some care in the intermediate region, where the peaks are highly distorted.

Trace *a* has a very low input intensity $\eta = 0.02$. On resonance, the average number of photons in the cavity is $n < 0.01$, more than two orders of magnitude less than the saturation photon number of the system $n_0 = 1.9$. We are probing the linear regime. Two peaks with the largest possible separation are clearly visible. Note that in Fig. 5 the heights are multiplied by a factor of 5 for the first three traces. The position of the peaks corresponds to the vacuum Rabi frequency Ω_{VR}. The modification in the peak position due to the decay rates κ and $\gamma_\perp$ is smaller than the uncertainties in the measurement. Scan *b* has an input intensity close to but below Y_{crit}, $\eta = 0.76$. Two changes are clearly visible: The position of the peaks has moved towards resonance ($\Omega = 0$) and the peaks are no longer Lorentzians, but show discontinuities. Scan *c* shows the transmission spectrum for an input intensity just above Y_{crit}, $\eta = 1.09$. At this point we see one symmetric peak centered on resonance. For scan *d* the intensity is well above Y_{crit}, $\eta = 1.84$. The number of photons inside the cavity on resonance is $n \approx 11\,000$, almost four orders of magnitude larger than the saturation photon number. The peak remains centered on resonance and the evolution from a well-defined doublet (trace *a*) to a singlet (trace *d*) is completed.

We now analyze the linewidths of the peaks. This is experimentally a more difficult issue than the peak positions since there are several mechanisms that do not affect the position but broaden the line. Throughout this discussion the expression ''linewidth'' refers to the full width at half maximum. Three traces (*a*, *c*, and *d*) out of the four marked in Fig. 5 present well-defined linewidths. For the low-intensity case (trace *a*), the vacuum Rabi sidebands have a measured linewidth of 8 ± 2 MHz; this agrees well with the theoretical value of 7.3 MHz, given by the average of the atomic and the cavity linewidths [real part of $\Omega_{1,2}$ in Eq. (14)].

The 30 ± 3 MHz linewidth of scan *c* is significantly larger than for any other value of the input intensity. This is the point where the two highly deformed vacuum Rabi peaks meet and form a combined peak (see Fig. 1). The linewidth at this point is not determined by the particular values of κ and $\gamma_\perp$ but by the coupling Ω_{VR}. A simple analytical expression can be obtained in the traveling plane-wave model, where the zero-phase condition results in a linewidth of $\sqrt{2}\Omega_{VR}$. Using the Gaussian standing-wave model, we find very good numerical agreement with the experimental observation.

The linewidth of trace *d* narrows to 10 ± 2 MHz. This is approaching the value of the empty cavity of 8.4 MHz. The line has a large pedestal recalling the presence of the atoms.

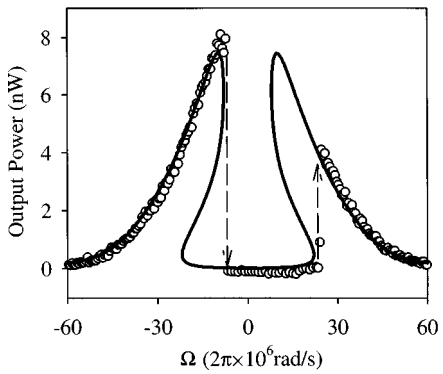

FIG. 6. Transmitted spectrum as a function of the excitation power for $\delta=0$. The frequency is scanned from below to above atomic resonance. The scan shown here is the same as trace *b* in Fig. 5. The parameters for the theoretical curve are $C=78$ and $(\kappa,\gamma_\perp,g_0)=(3.1,3.1,2.5)\times 2\pi\times 10^6$ rad/s.

Trace *b* (plotted separately in Fig. 6) shows a more complicated behavior. The trace is not symmetric with respect to resonance, even though the state equation is. This is caused by the multivaluedness of the anharmonic oscillators in this regime, as mentioned in the discussion of Fig. 1. The scan follows the upper branch of the frequency hysteresis while it approaches the center frequency. After jumping down at a fairly small negative laser detuning it stays on the lower branch, reaching a positive detuning of larger magnitude before it jumps up again. At this point the scan is already beyond the maximum value of the output intensity. The jumps are indicated by vertical dashed arrows. Our measurements show exactly this phenomenon. The difference in peak height and position corresponds very well to the theoretical prediction. The left peak is higher and closer to the center and the right peak is smaller and further away. Scanning in the opposite direction reverses the asymmetry establishing the frequency hysteresis. The peak shape is highly asymmetric due to the jumps from the upper to the lower branch of the hysteresis on the left and back to the upper branch on the right-hand side. We have scanned the spectrum in both directions and observed this hysteresis directly. The effect is very robust.

The complex transmission behavior of scan *b* is a manifestation of the fact that for the given parameters the steady state of the system is described by a complicated two dimensional manifold in the three-dimensional space shown in Fig. 5. In the transition region it is neither possible to define a linewidth nor appropriate to name the observed scan a ''spectrum'' since the nonlinearity of the two oscillators destroys these two concepts. The linewidth of the peak corresponds to the horizontal separation of two points on the shoulders of the peak. This is ill defined at this point since the inner (closer to resonance) shoulder is physically unstable (dotted curve). The spectrum does not exist because it requires the determination of a peak height at a point where the output intensity is multivalued.

All the scans shown in Fig. 5 correspond to projections of the state equation in vertical planes that are parallel to each other and parallel to the frequency axis. To gain additional understanding, we look at another projection: the vertical plane that is parallel to the input intensity axis and centered on the frequency axis. This is the projection of the complicated manifold that is usually shown in optical bistability.

TABLE I. Theoretical parameters for the figures ($\gamma_\parallel=6.2\times 2\pi\times 10^6$ rad/s).

Figure	$\Omega_{VR}/\gamma_\parallel$	$\kappa/\gamma_\parallel$	$\gamma_\perp/\gamma_\parallel$	X_{crit}	Y_{crit}
1,2	5.8	0.48	0.50	390	2500
6	6.3	0.50	0.50	450	2800
8,9	6.1	0.47	0.50	460	2900
10,11	5.3	0.32	0.61	390	2500
12,13	11.0	0.48	0.61	1500	8600

Figure 7 presents the transmission behavior of the system in this plane. These data were taken directly after the frequency scans shown in Fig. 5 by ramping the input intensity up and down with a frequency of 15 Hz while keeping the laser frequency on resonance with the atoms and the cavity and measuring the output intensity. The system is clearly bistable. The hollow dots *a*–*d* show the points where the corresponding scans from Fig. 5 penetrate this plane.

In the bistable region, the frequency scans do not go down to the lower branch. This is because these scans start at large-frequency detunings on the upper branch and then follow the upper branch all the way. The solution of the state equation in this region consists of two separate curves. The principle of the effect is visible in Fig. 1. Trace *A* is a broad peak; this solution is mapped out by the frequency scan. Trace *B* is a closed curve that lies underneath the broad peak disconnected from it. The bottom half of this closed curve is the lower branch of optical bistability, whereas the upper half presents an unstable solution. It is inviting to visualize the effect of the atoms on the transmission in the form of a cave that can be entered from the front by staying on resonance and changing the intensity, but not from the side [14].

From the ratio of the switching points we numerically determine the cooperativity *C* by using Eq. (7) and from that a value for the vacuum Rabi frequency through Eq. (6). The calculated frequency is larger than the one measured from trace *a* in Fig. 5 by a factor of 1.4. We observe this deviation consistently for all measurements reported in this paper. There are many mechanisms that are not considered in the theory presented in Sec. II that can lead to this deviation. A discussion of the effects of cavity imperfections, transit and Doppler broadening, and finite absorption is given in [28]. The effects of transit broadening are largest at the lower intensities. The inhomogeneous broadening in our system is small; transit and Doppler effects together increase the linewidth from 6.1 MHz to less than 8 MHz. Similar deviations have been observed by other groups [22] and they are not entirely unexpected. The model we use relies on the semiclassical limit of large atom and photon numbers. Our experiment does not fulfill the conditions of $C_1\rightarrow 0$ and $n_0\rightarrow\infty$. The frequency measurements are consistent, but there are deviations particularly in the intensities and the cooperativity as calculated from the OB properties. Table I shows the specific theoretical values used for the comparisons in the figures.

A comparison of the peaks of Fig. 5 shows quantitatively how the system evolves. We measure the values for the fre-

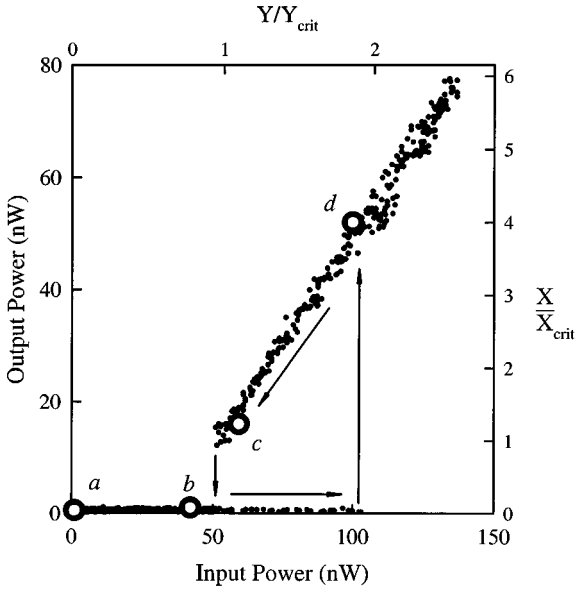

FIG. 7. Transmission on resonance with varying intensity. $\Omega=\delta=0$. The points a, b, c, and d mark where the frequency scans of Fig. 5 intersect with this plot.

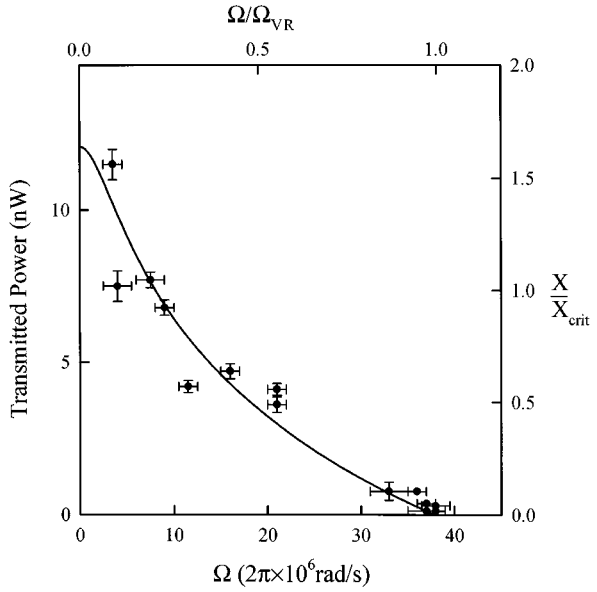

FIG. 9. Position of the sidebands as a function of output power. $\delta=0$. The solid curve is the zero-phase condition.

quencies and the input and the output intensities for the peaks on the lower-frequency side since this is the side where the scan reaches every point on the upper branch. Guided by the understanding of the model, we do not simply take the maximum peak heights, but we choose the value that is halfway between the maximum and the point where the scan jumps down to the lower branch. This allows us to compare the results with the zero-phase condition (16). Figure 8 shows the positions of the peaks depending on the input power. The solid curve marks the zero-phase condition. There are no adjustable parameters in this comparison. The left and the bottom axis show the absolute values. To facilitate comparison between runs with different parameters (see Figs. 12 and 13), we normalize the right and the top axis to critical values that are insensitive to the actual number of atoms. The frequency axis is normalized to the vacuum Rabi frequency Ω_{VR} and the input power axis is normalized to Y_{crit}.

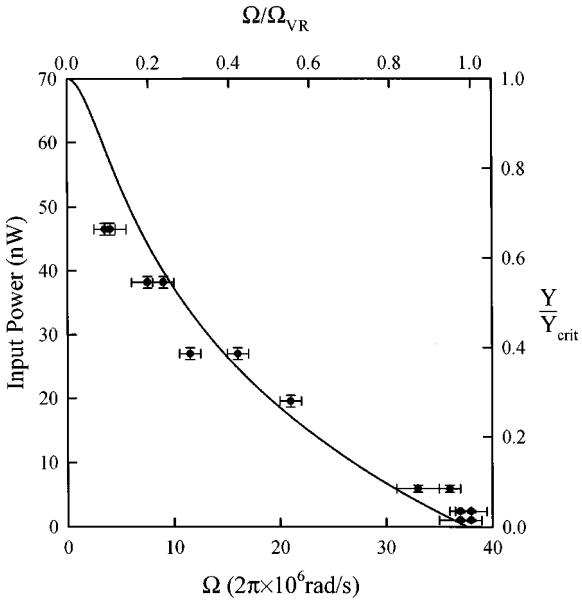

FIG. 8. Position of the sidebands as a function of input power. $\delta=0$. The solid curve is the zero-phase condition.

Since the detuning between atoms and cavity is zero, the behavior is symmetric and it is sufficient to plot only the side with positive laser detuning. The absolute input values have been scaled by a factor of 1.4 to optimize the fit.

Figure 9 is the equivalent to Fig. 8, showing the transmitted power instead of the input power. The absolute output values have been scaled by a factor of 1.8. Again we show only the positive half of the frequency axis since the graph is symmetric for zero atom-cavity detuning. Figures 8 and 9 show the growth of the transmission as the intensity increases, but also the shift of the peaks towards resonance as the system becomes more and more anharmonic.

B. Evolution with atom-cavity detuning

Figure 10 shows transmission spectra for different atom-cavity detunings at a low value of the input intensity ($\eta=0.01$). On resonance there are 0.002 photons in the cavity. The theoretical counterpart for this figure is Fig. 2. The three solid thick curves show the theoretical shape of the transmission derived from the state equation (7). The height has been scaled by a factor of 1.7 to optimize the fit. At this intensity level, the peaks are symmetric, an indication for the fact that the system is still in the linear regime. The two solid thin curves show the position of the peaks according to the zero-phase condition (16). The positions shift and the separation of the peaks increases for larger atom-cavity detunings. This is the signature of an avoided crossing (see Fig. 2) between the atomic transition and the resonant frequency of the cavity. There is good agreement in the position and the

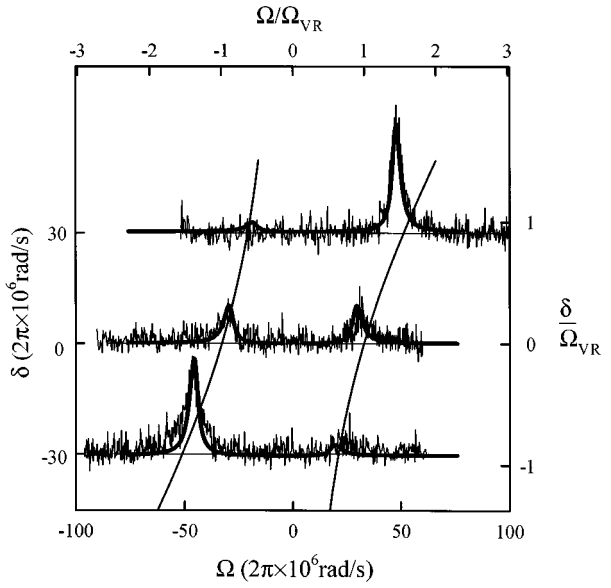

FIG. 10. Transmitted spectra for different atom-cavity detunings δ at very low input intensity. $P_{in}=0.5$ nW $=0.01P_{crit}$. The two tall peaks reach output powers of 0.2 nW.

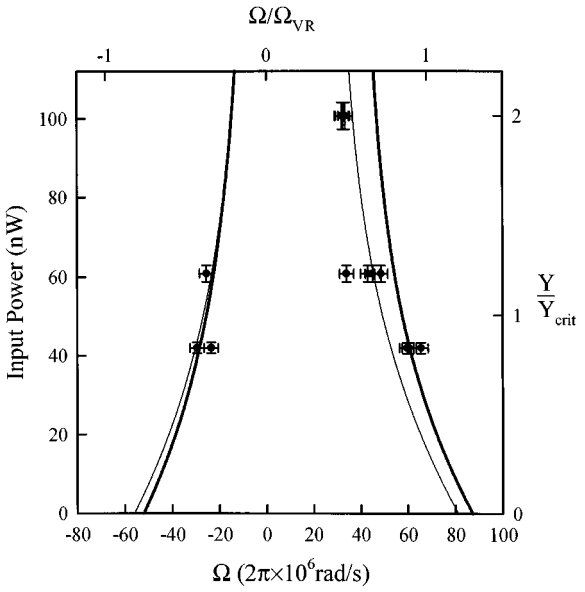

FIG. 12. Position of the sidebands depending on the input power. $\delta=(30\pm5)\times2\pi\times10^6$ rad/s. We show a theoretical band limited by this uncertainty; (thin, thick) curve $\delta=(25,35)\times2\pi\times10^6$ rad/s.

height ratios between data and theory. Due to limitations in the model, intensities are more likely subject to deviations than are frequencies. The laser versus atom-cavity detuning presentation shows precise agreement without any adjustments.

Figure 11 presents spectra at different atom-cavity detunings for intermediate values of the input intensity. Even though the number of photons on resonance inside the cavity is still fairly small (0.04), the nonlinear behavior is clearly visible in the asymmetry of the peaks. The theoretical curves in this plot have been shifted by 2 MHz or 0.06 Ω_{VR}, an amount that lies within the experimental systematic uncertainties in the frequency scaling. Again the height has been scaled by a factor of 1.7. Frequency hysteresis is not readily visible in the data while the theory, indicated by the solid curves, predicts a small amount. The peak heights and positions of the four larger peaks agree better with the theory than the heights and positions of the small peaks. This could be an indication for the higher sensitivity of the system to fluctuations when it is excited close to the atomic frequency.

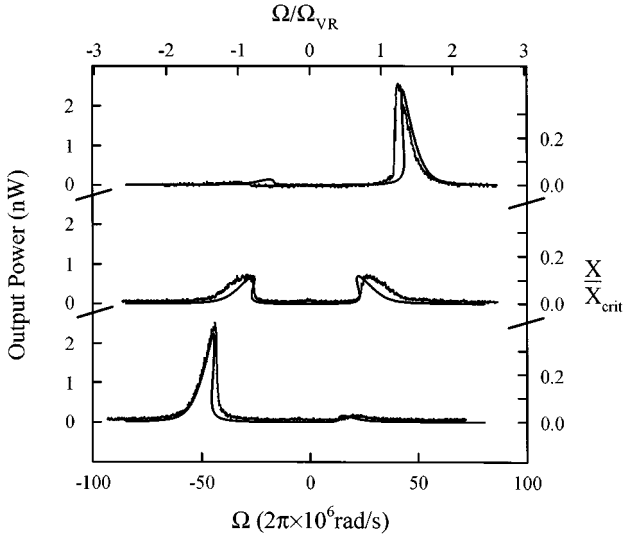

FIG. 11. Transmission spectra for different atom-cavity detunings at an intermediate input intensity. $P_{in}=7$ nW $=0.15P_{crit}$. The atom-cavity detunings for the three spectra from bottom to top are $(-29,\ 0,\ 32)\times2\pi\times10^6$ rad/s.

Figure 12 shows the positions of the peaks depending on the input intensity versus laser detuning. The theoretical intensity has been scaled by a factor of 0.52 to optimize the fit. The data shown in this figure were taken with a higher number of atoms than the data shown in Figs. 10 and 11, resulting in a larger separation of the sidebands. Since the scatter in the data is mainly due to the uncertainty in the value of the atom-cavity detuning, we show theoretical bands limiting the range to $\delta=(30\pm5)\times2\pi\times10^6$ rad/s. The uncertainty is a combination of the uncertainty in the laser frequency during the lock period of the data acquisition cycle and the typical drift and jitter of the cavity during the measurement period of the data acquisition cycle.

Figure 13 shows the positions of the peaks depending on the output intensity versus laser detuning. The theoretical intensity has been scaled by a factor of 1.4 to optimize the fit. Since we have no empty cavity scans available for the calibration of this particular set of measurements, we use the taller peak of a scan with large atom-cavity detuning, so that the peak height depends only weakly on the precise values of the parameters, and calculate the transmission from the state equation (7). Using this transmission and the calibration of the input power, we get a calibration of the output power.

Figure 12 corresponds to Fig. 8, but with a positive atom-cavity detuning of $\delta=30\times2\pi\times10^6$ rad/s. The behavior is no longer symmetric. We observe an overall shift of the

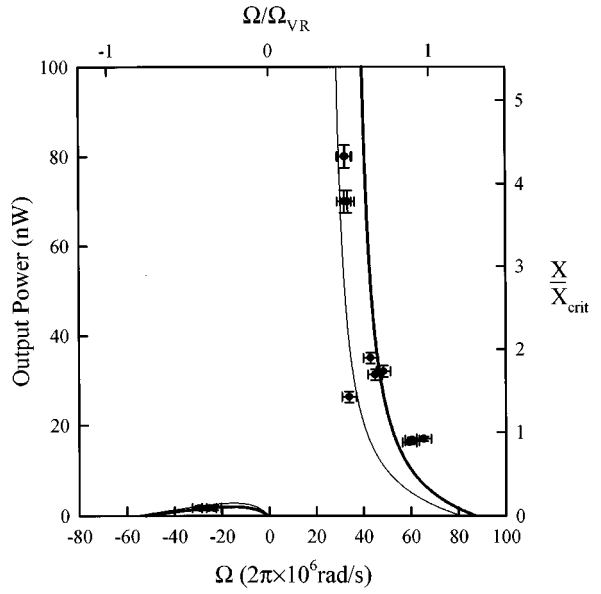

FIG. 13. Position of the sidebands depending on the output power. $\delta=(30\pm5)\times2\pi\times10^6$ rad/s. We show a theoretical band limited by this uncertainty; (thin, thick) curve $\delta=(25,35)\times2\pi\times10^6$ rad/s.

peaks towards positive laser detuning. This is a manifestation of the avoided crossing as observed for low intensities in Fig. 11. We see good agreement between data and theory. Both uncertainty and scatter of the data are smaller on the side of negative laser detuning and larger on the side of positive detuning.

Figure 13 is the nonresonant equivalent of the resonant data in Fig. 9. The peaks are shifted to higher laser detunings as expected, since this shows the same data as Fig. 12. The effect of the avoided crossing appears in this figure in the same way, but with the added information of the transmission.

The difference in the output intensity between the resonant and the nonresonant data shows how this nonlinear oscillator driven off resonance suppresses the transmission of the sideband that is closer to the atomic frequency. The behavior of the peak with positive laser detuning (closer to ω_c) still bears resemblance to the on-resonant system: It moves closer to resonance and grows when the driving intensity increases. On the side of negative laser detuning (closer to ω_a) the picture changes completely. Instead of growing, the peak height stays constant; only the position moves. Here the properties of a coupled system balance with those of a decoupled system. The shift of the peak position is due to the former atom-cavity entity creating two nonlinear oscillators. The suppression of the peak is due to the latter as we have an avoided crossing. Now atoms and cavity act differently on the transmission.

V. CONCLUSION

We have characterized the transmission properties of an optical atom-cavity system as a function of excitation intensity and frequency in detail. Two normal modes, the vacuum Rabi sidebands, are present in the transmission spectrum at low intensity of the driving field due to the coupling between atoms and cavity field. We have gradually decoupled the atoms and cavity from each other in different ways and have mapped out the region where the transition from the coupled to the uncoupled system takes place. The amount and quality of the data allowed a detailed analysis in this transition region.

In the on-resonance case, we have observed quantitatively an anharmonic evolution from the two vacuum Rabi peaks in the low-intensity regime to the single transmission peak in the high-intensity limit. This shows how the system decouples for increasing driving intensities; the atoms saturate and the behavior of the system resembles that of an empty cavity. In the transition region, the vacuum Rabi peaks shift and deform and the transmission exhibits multistable behavior. This frequency hysteresis is clearly visible in our data and agrees with theoretical predictions. The absolute quantitative agreement with the intensities is within a factor of 2. The most important reason for this disagreement is probably the failure of the semiclassical limit. However, when the intensities are scaled by the critical intensities, the agreement is very good, pointing to a simple scaling factor that at this time we cannot fully explain in terms of uncertainties in the measurement.

We have also observed the decoupling due to an increase of the detuning between atoms and cavity. The avoided crossing between atoms and cavity appeared in our measurements for low intensities and even for intermediate intensities the basic structure remained and agreed well with the theoretical predictions. The decoupling caused a shift of the normal modes towards the characteristic frequencies of the uncoupled system as well as a change in the peak heights. The peak heights are affected differently since the cavity enhances transmission at its characteristic frequency, whereas the atoms suppress it.

Finally, we have probed a region of parameter space where we gradually decoupled atoms and cavity using high intensity and atom-cavity detuning. The atom-cavity system showed a balance between the effects of a coupled system (a frequency shift of anharmonic oscillators) and the effects of an uncoupled system (suppression of the transmission due to atomic absorption).

Although the presented results can be interpreted as transmission spectra, this is only true in the low-intensity limit. The observed anharmonicity and frequency hysteresis provide a link between the predictions of cavity QED and the semiclassical theory of OB. They are the semiclassical counterpart of the multiphoton resonances in the energy-level structure of an atom-cavity system [14] seen in cavity QED. The direct spectral observation of these resonances in the optical regime remains elusive, but there are proposals for overcoming the difficulties [29].

ACKNOWLEDGMENTS

We wish to thank H. J. Carmichael for helpful discussions and G. T. Foster for experimental assistance. J. G. acknowledges support from the Studienstiftung des Deutschen Volkes. This work was supported by the National Science Foundation and equipment loans from the Northrop-Grumman Corporation.

[1] E. T. Jaynes and F. W. Cummings, Proc. IEEE **51**, 89 (1963).
[2] J. J. Sánchez Mondragón, N. B. Narozhny, and J. H. Eberly, Phys. Rev. Lett. **51**, 550 (1983).
[3] G. S. Agarwal, Phys. Rev. Lett. **53**, 1732 (1984).
[4] L. A. Lugiato, in *Progress in Optics*, edited by E. Wolf (North-Holland, Amsterdam, 1984), Vol. XXI, p. 69.
[5] *Cavity Quantum Electrodynamics*, edited by Paul R. Berman (Academic, San Diego, 1994).
[6] Y. Kaluzny, P. Goy, M. Gross, J. M. Raimond, and S. Haroche, Phys. Rev. Lett. **51**, 1175 (1983).
[7] R. J. Brecha, L. A. Orozco, M. G. Raizen, M. Xiao, and H. J. Kimble, J. Opt. Soc. Am. B **3**, 238 (1986); **12**, 2329 (1995).
[8] M. G. Raizen, R. J. Thompson, R. J. Brecha, H. J. Kimble, and H. J. Carmichael, Phys. Rev. Lett. **63**, 240 (1989).
[9] Yifu Zhu, Daniel J. Gauthier, S. E. Morin, Qilin Wu, H. J. Carmichael, and T. W. Mossberg, Phys. Rev. Lett. **64**, 2499 (1990).
[10] R. J. Thompson, G. Rempe, and H. J. Kimble, Phys. Rev. Lett. **68**, 1132 (1992).
[11] J. J. Childs, K. An, M. S. Otteson, R. R. Dasari, and M. S. Feld, Phys. Rev. Lett. **77**, 2901 (1996).
[12] S. L. Mielke, G. T. Foster, J. Gripp, and L. A. Orozco, Opt. Lett. **22**, 325 (1997).
[13] H. J. Carmichael, Phys. Rev. A **33**, 3262 (1986).
[14] J. Gripp, S. L. Mielke, L. A. Orozco, and H. J. Carmichael, Phys. Rev. A **54**, R3746 (1996).
[15] M. Brune, F. Schmidt-Kaler, A. Maali, J. Dreyer, E. Hagley, J. M. Raimond, and S. Haroche, Phys. Rev. Lett. **76**, 1800 (1996).
[16] D. M. Meekhof, C. Monroe, B. E. King, W. M. Itano, and D. J. Wineland, Phys. Rev. Lett. **76**, 1976 (1996).
[17] See, for example, C. Weisbuch, M. Nishioka, A. Ishikawa, and Y. Arakawa, Phys. Rev. Lett. **69**, 3314 (1992); H. Cao, J. Jacobson, G. Björk, S. Pau, and Y. Yamamoto, Appl. Phys. Lett. **66**, 1107 (1995).
[18] J. Gripp, S. L. Mielke, and L. A. Orozco, Phys. Rev. A **51**, 4974 (1995).
[19] C. W. Gardiner and A. S. Parkins, Phys. Rev. A **50**, 1792 (1994).
[20] P. Kochan and H. J. Carmichael, Phys. Rev. A **50**, 1700 (1994).
[21] P. D. Drummond, IEEE J. Quantum Electron. **QE-17**, 301 (1981).
[22] G. Rempe, R. J. Thompson, R. J. Brecha, W. D. Lee, and H. J. Kimble, Phys. Rev. Lett. **67**, 1727 (1991).
[23] K. An, J. J. Childs, R. R. Dasari, and M. S. Feld, Phys. Rev. Lett. **73**, 3375 (1994).
[24] J. Gripp and L. A. Orozco, Quantum Semiclassic. Opt. **8**, 823 (1996).
[25] M. Raizen, Ph.D. dissertation, University of Texas at Austin, 1989 (unpublished).
[26] J. Gripp, Ph.D. dissertation, State University of New York at Stony Brook, 1997 (unpublished).
[27] R. W. P. Drever, J. L. Hall, F. V. Kowaski, J. Hough, G. M. Ford, A. J. Munley, and H. Ward, Appl. Phys. B **31**, 97 (1983); J. L. Hall, L. Hollberg, T. Baer, and H. G. Robinson, Appl. Phys. Lett. **39**, 680 (1981).
[28] A. T. Rosenberger, L. A. Orozco, H. J. Kimble, and P. D. Drummond, Phys. Rev. A **43**, 6284 (1991).
[29] H. J. Carmichael, P. Kochan, and B. C. Sanders, Phys. Rev. Lett. **77**, 631 (1996).